APL MATERIALS **2**, 096103 (2014)

Fabrication of piezodriven, free-standing, all-oxide heteroepitaxial cantilevers on silicon

N. Banerjee, E. P. Houwman, G. Koster,[a] and G. Rijnders
Faculty of Science and Technology and MESA+ Institute for Nanotechnology, University of Twente, P.O. Box 217, 7500 AE Enschede, The Netherlands

(Received 23 March 2014; accepted 6 August 2014; published online 3 September 2014)

We report on the fabrication and mechanical properties of all-oxide, free-standing, heteroepitaxial, piezoelectric, microelectromechanical systems (MEMS) on silicon, using $PbZr_{0.52}Ti_{0.48}O_3$ as the key functional material. The fabrication was enabled by the development of an epitaxial lift-off strategy for the patterning of multilayer oxide heterostructures grown on Si(001), employing a high temperature stable, sacrificial oxide template mask to obtain freestanding cantilever MEMS devices after substrate etching. All cantilevers, with lengths in the range 25–325 μm, width 50 μm, and total thickness of 300 nm, can be actuated by an external AC-bias. For lengths 50–125 μm, the second order bending mode formed the dominant resonance, whereas for the other lengths different or multiple modes were present. © *2014 Author(s). All article content, except where otherwise noted, is licensed under a Creative Commons Attribution 3.0 Unported License.* [http://dx.doi.org/10.1063/1.4893355]

Piezoelectric microelectromechanical systems (MEMS) devices have attracted remarkable interest in recent times for their ability to convert between electrical and mechanical energy, which is crucial for many potential applications. Among the different piezoelectric materials, $PbZr_{1-x}Ti_xO_3$ (PZT), specifically the composition with x = 0.48 has been extensively applied because of its very large electro-mechanical coupling and stable polarization response on external perturbations.[1] Compared to electrostatic MEMS, piezoelectric devices offer advantages in larger actuation amplitude, a faster response time and lower operation voltage. Consequently, PZT has been utilized as active piezoelectric component in many electromechanical devices, such as mass sensors,[2] energy harvesters,[3] accelerometers,[4] force sensors,[5] actuators,[6] and micro-pumps.[7] PZT is a complex solid solution oxide material and is very stable with respect to different physical and chemical structuring processes.[8] It was shown that PZT's properties can be optimally used in all oxide devices[9] but major challenges are faced when incorporating heteroepitaxial PZT in very large scale integration (VLSI) technology with Si for micro-fabrication of piezo-electromechanical components.[8,10]

Many of the piezoelectric MEMS devices have a cantilever configuration, operating in bending mode. They generate an open circuit voltage when deformed, as well as manifest mechanical actuation in response to an external voltage, and hence can be employed for both sensing and actuation purposes. Such devices typically consist of an active piezoelectric film fabricated on a thin Si beam, which is capable of free vertical movement. An external bias induces a lateral extension or contraction in the piezoelectric layer, causing a bimorph actuation due to the clamping with the substrate and/or asymmetries between the electrode layers. Very accurate sensing can also be realized by bringing the cantilever into a resonant state by applying an alternating electrical bias voltage with appropriate frequency. For example in the mass sensor any change in the cantilever mass (Δm) alters the resonance frequency (f_n) and measurement of the frequency shift (Δf_n) offers the possibility to measure the mass change very accurately. This label-free mass-sensing and measurement principle is utilized for a wide range of applications from bio-chemical,[11] biological[12] to even atomic physics.[13]

[a]Author to whom correspondence should be addressed. Electronic mail: g.koster@utwente.nl

 ©Author(s) 2014

This article is copyrighted as indicated in the article. Reuse of AIP content is subject to the terms at: http://aplmaterials.aip.org/about/rights_and_permissions Downloaded to IP: 130.89.23.40 On: Wed, 25 Mar 2015 20:47:14

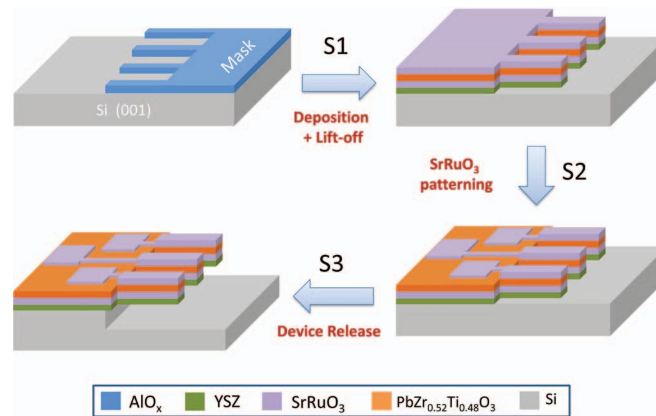

FIG. 1. Schematic representation of the fabrication process. The Si (001) substrate is masked with a structured amorphous AlO_x layer. Step S1: Deposition of heteroepitaxial oxides followed lift-off of the sacrificial AlO_x mask, resulting in multilayer structuration. Step S2: Patterning of the epitaxial top electrode. Step S3: Anisotropic chemical etching of Si to achieve free-standing piezo-MEMS devices.

The bending resonance frequencies (f_n) of a cantilever of length L, width W, thickness t with (effective) Young's modulus E, and beam mass per length m_L (density ρ_c), are given by[14] (under the condition $L \geq W \gg t$),

$$f_n = \frac{\alpha_n^2}{2\pi L^2}\sqrt{\frac{E(Wt^3/12)}{m_L}} = \frac{\alpha_n^2 t}{2\pi L^2}\sqrt{\frac{E}{12\rho_c}} = \frac{C_1 t}{L^2}. \tag{1}$$

Here α_n are numerical factors, increasing with n ($\alpha_1 = 1.875$ for the fundamental mode, $\alpha_2 = 4.69$ for the second order mode) and C_1 comprises all parameters that do not depend on the size of the beam. The mass sensitivity, $S_m = \Delta f_n/\Delta m = -f_n/2m_L L$,[14(a),15] written in terms of dimensional parameters, $S_m = -C_1/(\rho_c L^3 W)$, is independent of device thickness. To increase S_m, one has to decrease the lateral dimensions of the cantilever, but in order to maintain bending mode operation, the cantilever should also be sufficiently thin. Hence, the first step towards miniaturizing the cantilever is the development of a technique capable of reducing the cantilever thickness with the possibility of further reduction of the beam area.

Free-standing devices of relaxor materials can lead to enhanced functional properties.[16] However, investigations into free-standing epitaxial PZT devices have remained elusive up till now, mainly due to difficulties in the fabrication. In traditional piezo-MEMS technology devices are fabricated using silicon on insulator (SOI) wafers.[17] Because of the different physical and chemical nature of the individual oxide layers of an oxide cantilever, one requires multiple lithography steps to fabricate a device based on a SOI substrate, using back-etch structuring.

In this report, we demonstrate the fabrication of all-oxide, heteroepitaxial, freestanding, cantilever-based PZT MEMS devices on Si (001) substrate, using a single step *lift-off structuring* process. Si substrates were used instead of SOI, requiring minimal front-side etching of the Si only. The electromechanical resonating behavior of these cantilevers has been investigated as function of the cantilever length.

The all-oxide, heteroepitaxial free-standing devices were fabricated using an oxide lift-off patterning technique for the epitaxial multilayer heterostructure, followed by anisotropic substrate etching. The high temperature grown oxide multilayer stack, incorporating the buffer layer, the bottom and top oxide electrode layers and the functional PZT layer, was structured via a single step epitaxial lift-off process recently developed.[18] The process is shown in Fig. 1. A layer of amorphous aluminum oxide (AlO_x) was used as a high temperature stable, sacrificial lift-off mask. The mask layer was grown on a Si(001) substrate via pulsed laser deposition (PLD) at room temperature. It was structured via conventional photolithography, where the alkaline photoresist developer solution also acts as the etchant for the AlO_X layer. Details of the procedure can be found in Ref. 18. Next

This article is copyrighted as indicated in the article. Reuse of AIP content is subject to the terms at: http://aplmaterials.aip.org/about/rights_and_permissions Downloaded to IP: 130.89.23.40 On: Wed, 25 Mar 2015 20:47:14

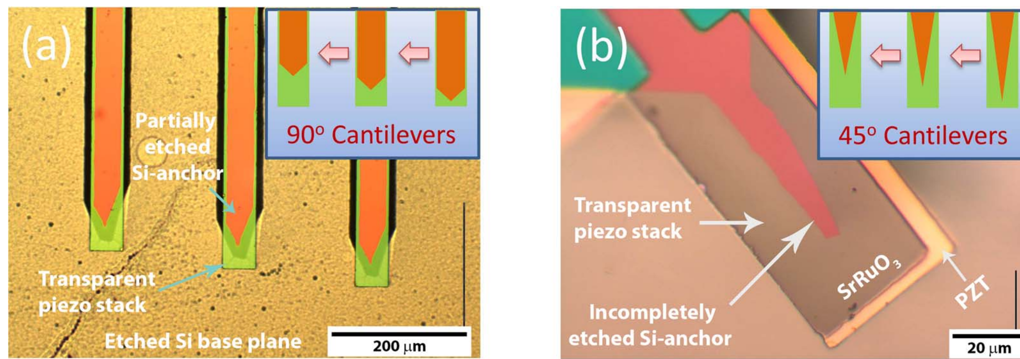

FIG. 2. Optical microscopic images (top view) of partially etched cantilevers, aligned (a) perpendicular and (b) 45° to the Si substrate [001] crystal axis. The insets show schematically the gradual retraction of the anchor during KOH etching in both cases.

the functional oxide layers were deposited at high temperatures by PLD. Yttria stabilized zirconia (YSZ) was employed as the buffer layer (here ∼100 nm) on Si which facilitated subsequent epitaxial perovskite growth, because it scavenges the native oxide on the substrate surface.[19] In the final device, the YSZ layer also enhances bi-morph actuation of the piezo-layer because it causes an asymmetry of the heterostructure. A multilayer of PZT (∼150 nm) sandwiched between $SrRuO_3$ (SRO) electrodes (∼25 nm) was subsequently PLD grown at high (600 °C) temperature under optimized growth conditions.[20] However, on top of the AlO_x mask layer the growth is polycrystalline. After controlled annealing under high oxygen pressure, the AlO_x mask, together with the amorphous oxide layers were lifted-off using a 2M NaOH solution, patterning the entire heteroepitaxial multilayered oxide assembly. The SRO top electrode layer was patterned via photolithography and dry Ar-ion etching. Lift-off removal of the sacrificial AlO_x mask gives direct access to the Si substrate. Anisotropic hot KOH-etching was employed to etch selectively the Si(001) substrate, releasing the all-oxide, free-standing epitaxial cantilevers. The fabricated cantilevers were characterized using optical and electron microscopy. Ferroelectric behavior of unreleased devices was measured with an aixACCT analyzer TF2000. The electromechanical response of the PZT cantilevers was investigated employing laser Doppler vibrometry, using an AC-field $E_{tt}\cong$7kV/cm at a DC bias field of 200 kV/cm.

X-ray diffraction of the patterned multilayers showed reflections consistent with (110)-oriented growth only, proving that all oxides layers are epitaxial, crystalline and identical to those on an unmasked substrate.[21] No diffraction signal was observed from the AlO_x layer indicating its complete removal. We have investigated two different orientations: (i) cantilevers which were oriented perpendicular to the Si[100] in plane crystal axis ("90° cantilevers" shown in Fig. 2(a) after partial Si etching), and (ii) cantilevers which were oriented 45° with respect to that axis ("45° cantilevers" shown in Fig. 2(b)). Because of the anisotropic etching of Si the 45° cantilevers displayed a much faster release than 90° cantilevers. The differential etching behavior also affects the geometry of Si anchor of the cantilever. The 45° cantilevers had minimal undercut and were used for all experiments described here. Fig. 3(a) provides an overview SEM image of a series of devices with different cantilever lengths, showing also the contact pads to the SRO top-electrode. Since the thin (∼300 nm) oxide stack is transparent, the different functional oxide layers (see Fig. 2(b)) and the triangular Si substrate anchor can be clearly identified in the optical images of an array (Fig. 3(b)) and a single cantilever (Fig. 3(c)). Fig. 3(d) gives a side-view SEM image of a representative cantilever, proving that the non-actuated device has no noticeable curvature, which is usually present in Si-based cantilevers due to thermal expansion mismatch.

The room temperature ferroelectric response (current-voltage behavior and corresponding polarization-electric field hysteresis loop) of a representative cantilever device (area = 100 × 100 μm^2) before substrate etching is shown in Fig. 4. The loop is very symmetric, with a coercive field of ∼85 kV/cm. The remnant and saturation polarizations are ∼24 $\mu C/cm^2$ and ∼35 $\mu C/cm^2$, respectively. The ferroelectric response was stable up to at least the maximum applied number of

This article is copyrighted as indicated in the article. Reuse of AIP content is subject to the terms at: http://aplmaterials.aip.org/about/rights_and_permissions Downloaded to IP: 130.89.23.40 On: Wed, 25 Mar 2015 20:47:14

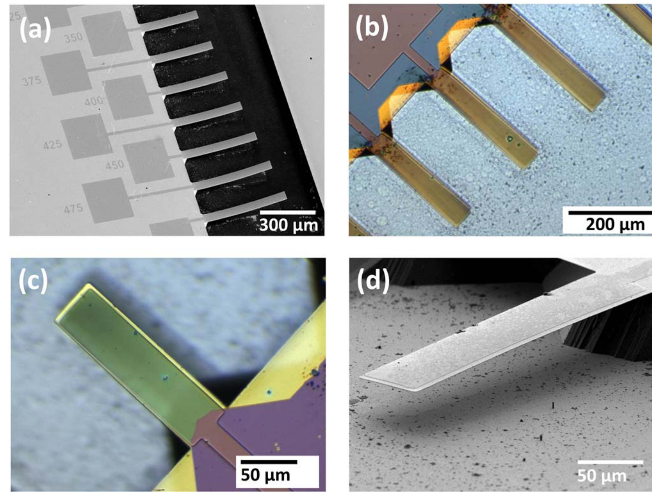

FIG. 3. (a) SEM overview of a series of cantilevers with different lengths. (b) and (c) Top-view optical microscopic images of a series of and a single cantilever device, respectively, showing the triangular substrate anchor. (d) Side-view SEM image of a single cantilever proving that the post-etched devices were free-standing and flat.

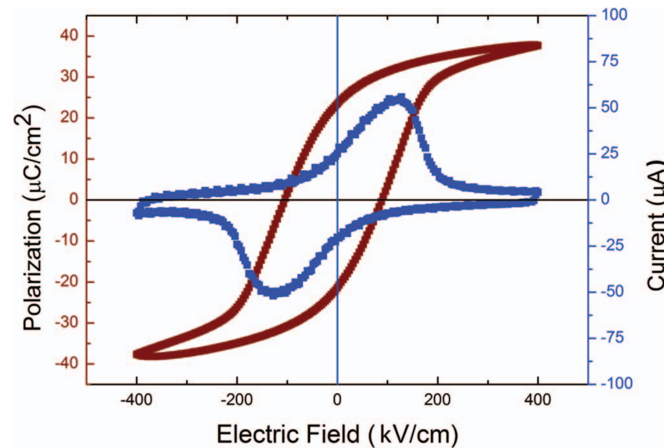

FIG. 4. Current-electric field behavior (blue) and corresponding polarization-field loop (brown) at 1000 Hz (top-bottom measurement in capacitor configuration) for 150 nm thick ferroelectric $PbZr_{0.52}Ti_{0.48}O_3$ epitaxial film on $SrRuO_3$/YSZ/Si(001).

10^8 switching cycles (because of the epitaxial electrodes used). After substrate etching the device cannot be cycled anymore to high voltages, because of damage due to the large piezo-electric stresses. This well-behaved ferroelectric response shows that the patterning strategy does not affect the ferroelectric properties of perovskite heterostructures.[18] Using the procedure described in Ref. 22, the effective piezoelectric coefficient $d_{31,\,\mathrm{eff}} = -115$ pm/V was determined from a 50 μm long, piezodriven freestanding cantilever. The obtained value corresponds well with the value found for piezodriven Si-based cantilevers.[22]

Fig. 5 shows the measured resonance frequency (f_{res}) of the mode with the highest resonance amplitude (in ambient conditions) versus the cantilever length. The dashed curve shown is the theoretical fit of the measured data in the length range $L = 50$–325 μm (given by filled circles), according to Eq. (1) with calculated $C_1 = 4950$ (Hz m) using average $E = 1.16 \times 10^{11}$ N/m^2 and $\rho_c = 6.7 \times 10^3$ kg/m^3 for the oxide stack, which shows that f_{res} is fairly well described by the second order bending mode. For the shortest beam with 25 μm length (open circle), the L/W aspect ratio is less than one. Here, the observed dominant mode was a vibrational mode over the width of the cantilever, with a corresponding lower resonance frequency. The inset shows the tip resonance amplitude versus frequency spectrum, of a representative freestanding cantilever

This article is copyrighted as indicated in the article. Reuse of AIP content is subject to the terms at: http://aplmaterials.aip.org/about/rights_and_permissions Downloaded to IP: 130.89.23.40 On: Wed, 25 Mar 2015 20:47:14

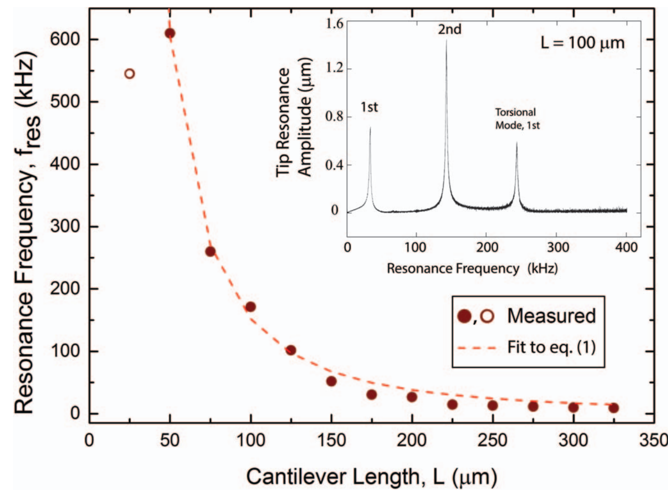

FIG. 5. Measured dependence of the resonance frequency of the dominant mode on the length of the freestanding heteroepitaxial cantilevers (with constant width of 50 μm), shown by symbols. The broken line represents a theoretical fit according to Eq. (1), to the experimentally measured data, excluding $L = 25$ μm which is shown by the open circle. The inset shows a representative tip resonance amplitude versus frequency spectrum for a cantilever with length 100 μm.

($LxW = 100$ μm $\times$ 50 μm), proving that the second harmonic mode is the dominant resonance. According to Eq. (1), $f_{res}L^2$ of the second order mode is expected to be a constant, independent of cantilever length. We also note that the first order bending mode has shifted to higher resonance frequency than expected. The dependence of $f_{res}L^2$ on the length of the cantilever is presented in Fig. 6 for devices with constant total thickness of 300 nm and width $W = 50$ μm. Four different regimes can be distinguished in this graph: $L < 50$ μm, 50 μm $\leq L \leq$ 150 μm, a transition region 150 μm $\leq L \leq$ 200 μm and the range with larger L. The inset shows the measured shape of a 50 μm cantilever in resonance, corresponding to the expected shape for a second order bending mode. Constant value fitting was adopted to the range 50 μm $\leq L \leq$ 150 μm to extract $C_1 = 5240$ (Hz m). This value is 6% larger than the calculated value. We ascribe the somewhat increased value of C_1 to the effect of the pyramid shape of the anchor of these cantilevers (see Fig. 3(c)). It was observed that this causes a slight curvature over the width of the beam near the anchor, increasing the effective spring constant of the beam, which can be interpreted as an increased Young's modulus. The scatter of the value of $f_{res}L^2$ in this range may then be due to variation of the anchor shape, caused by local variations in the etching speed. We conclude that in this range the cantilevers oscillate in a pure bending mode. The appearance of the second order mode as the dominant resonance is presumably originating from the asymmetric clamping by the triangular substrate base. We think that the resonance frequency of the first order bending mode is even more sensitive to the shape of the anchor, therefore enhancing the effective stiffness and thus the resonance frequency of the beam for this mode. Since the cantilevers were very thin and flexible, higher order mode are easily excited. For larger lengths the C_1 value drops significantly. Above a length of 175 μm, the cantilevers become progressively flexible and the cantilevers do not oscillate in a single flexural mode, but that also other resonances are present. These modes can absorb part of the supplied energy. The second inset in Fig. 6 shows the resonance profile of a 300 μm beam. This profile could not be fitted with a single bending mode, which demonstrates the presence of mixed modes in longer freestanding cantilevers.

In conclusion, free-standing heteroepitaxial all-oxide piezo-MEMS cantilever devices, with PZT as active layer, were fabricated directly on Si(001) substrates without the use of a SOI wafer and backside etching. A sacrificial oxide mask was used in an epitaxial lift-off structuring process to achieve patterning of the heteroepitaxial oxide layer stack deposited at high temperatures. Selective area, anisotropic front side etching of the substrates was employed for release of the devices. The structured devices show well-behaved ferro and piezo-electric responses. A dominant second order resonant bending mode was observed for devices with $L = 50$–125 μm. For the other lengths different or multiple modes were excited. The combined structuration strategy for the entire oxide

This article is copyrighted as indicated in the article. Reuse of AIP content is subject to the terms at: http://aplmaterials.aip.org/about/rights_and_permissions Downloaded to IP: 130.89.23.40 On: Wed, 25 Mar 2015 20:47:14

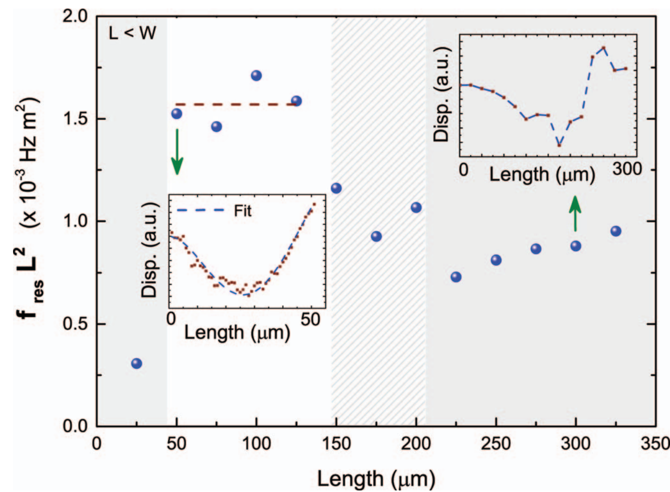

FIG. 6. Measured variation of $f_{res}L^2$ as function of the length for cantilevers with constant width $W = 50\ \mu$m and thickness $t = 300$ nm. Different regions of the obtained values are shaded in the graph. Constant value ($C_1 t$) fitting was applied to the data in the range $L = 50$–$125\ \mu$m (broken lines). Displacement vs length profile at resonance for representative cantilevers with $L = 50\ \mu$m and $L = 300\ \mu$m are shown in the insets.

multilayer stack down to the substrate can pave the way for integrating functional perovskite oxide heteroepitaxial multilayers in VLSI technology. The fabrication of free-standing cantilevers without any residual Si layer on the bottom opens up the possibility to achieve very high mass sensitivity by further reduction in cantilever surface area. The influence of the beam length on the damping behavior of free standing cantilevers arising from intrinsic (material dependent) properties and from the operational medium is subject of further study.

This research was carried out under Project No. M62.2.08SDMP21 in the framework of the Industrial Partnership Program on Size Dependent Material Properties of the Materials innovation institute M2i (www.m2i.nl) and the Foundation of Fundamental Research on Matter (FOM) (www.fom.nl), which is part of the Netherlands Organization for Scientific Research (www.nwo.nl). It was also supported by NanoNextNL of the Dutch Government and 130 partners.

[1] E. Cross, "Materials science: Lead-free at last," Nature (London) **432**(7013), 24–25 (2004).
[2] Y. Lee, G. Lim, and W. Moon, "A self-excited micro cantilever biosensor actuated by PZT using the mass micro balancing technique," Sens. Actuat. A **130–131**, 105–110 (2006).
[3] S. Saadon and O. Sidek, "A review of vibration-based MEMS piezoelectric energy harvesters," Energy Convers. Manag. **52**(1), 500–504 (2011).
[4] Y. Nemirovsky, A. Nemirovsky, P. Muralt, and N. Setter, "Design of novel thin-film piezoelectric accelerometer," Sens. Actuat. A **56**(3), 239–249 (1996).
[5] C. Lee, T. Itoh, and T. Suga, "Micromachined piezoelectric force sensors based on PZT thin films," IEEE Trans. Ultrason., Ferroelect. Freq. Control **43**(4), 553–559 (1996).
[6] A. Moskalik, "Piezoelectric actuation: State of the art," Shock Vibrat. Digest **33**, 269 (2001).
[7] R. M. White, "Silicon-based ultrasonic microsensors and micropumps," Integrat. Ferroelect. **7**(1–4), 353–358 (1995).
[8] P. Muralt, "PZT thin films for microsensors and actuators: Where do we stand?," IEEE Ultrason., Ferroelect. Freq. Control **47**(4), 903–915 (2000).
[9] C. Eom, R. Van Dover, J. M. Phillips, D. Werder, J. Marshall, C. Chen, R. Cava, R. Fleming, and D. Fork, "Fabrication and properties of epitaxial ferroelectric heterostructures with (SrRuO3) isotropic metallic oxide electrodes," Appl. Phys. Lett. **63**(18), 2570–2572 (1993).
[10] P. Muralt, N. Ledermann, J. J. Baborowski, and S. Gentil, "Integration of piezoelectric Pb(ZrxTi1-x)O-3 (PZT) thin films into micromachined sensors and actuators," Microsystems **9**, 1–24 (2002).
[11] T. Y. Kwon, K. Eom, J. H. Park, D. S. Yoon, T. S. Kim, and H. L. Lee, "In situ real-time monitoring of biomolecular interactions based on resonating microcantilevers immersed in a viscous fluid," Appl. Phys. Lett. **90**(22), 223903 (2007).
[12] A. Janshoff, H.-J. Galla, and C. Steinem, "Piezoelectric mass-sensing devices as biosensors: An alternative to optical biosensors?," Angew. Chem. Int. Ed. **39**, 4004–4032 (2000).
[13] Y. Yang, C. Callegari, X. Feng, K. Ekinci, and M. Roukes, "Zeptogram-scale nanomechanical mass sensing," Nano Lett. **6**(4), 583–586 (2006).

This article is copyrighted as indicated in the article. Reuse of AIP content is subject to the terms at: http://aplmaterials.aip.org/about/rights_and_permissions Downloaded to IP: 130.89.23.40 On: Wed, 25 Mar 2015 20:47:14

[14] (a) J. Tamayo, P. M. Kosaka, J. J. Ruz, Á. San Paulo, and M. Calleja, "Biosensors based on nanomechanical systems," Chem. Soc. Rev. **42**(3), 1287–1311 (2013); (b) A. W. McFarland, M. A. Poggi, L. A. Bottomley, and J. S. Colton, "Characterization of microcantilevers solely by frequency response acquisition," J. Micromech. Microeng. **15**(4), 785 (2005).
[15] N. V. Lavrik and P. G. Datskos, "Femtogram mass detection using photothermally actuated nanomechanical resonators," Appl. Phys. Lett. **82**(16), 2697–2699 (2003).
[16] S. H. Baek, J. Park, D. M. Kim, V. A. Aksyuk, R. R. Das, S. D. Bu, D. A. Felker, J. Lettieri, V. Vaithyanathan, S. S. N. Bharadwaja, N. Bassiri-Gharb, Y. B. Chen, H. P. Sun, C. M. Folkman, H. W. Jang, D. J. Kreft, S. K. Streiffer, R. Ramesh, X. Q. Pan, S. Trolier-McKinstry, D. G. Schlom, M. S. Rzchowski, R. H. Blick, and C. B. Eom, "Giant piezoelectricity on Si for hyperactive MEMS," Science **334**(6058), 958–961 (2011).
[17] M. D. Nguyen, H. Nazeer, K. Karakaya, S. Pham, R. Steenwelle, M. Dekkers, L. Abelmann, D. Blank, and G. Rijnders, "Characterization of epitaxial Pb (Zr, Ti) O3 thin films deposited by pulsed laser deposition on silicon cantilevers," J. Micromech. Microeng. **20**(8), 085022 (2010).
[18] N. Banerjee, G. Koster, and G. Rijnders, "Submicron patterning of epitaxial PbZr0.52Ti 0.48O3 heterostructures," Appl. Phys. Lett. **102**(14), 142909 (2013).
[19] S. Wang, C. Ong, L. You, and S. Xu, "Epitaxial growth of yittria-stabilized zirconia oxide thin film on natively oxidized silicon wafer without an amorphous layer," Semicond. Sci. Technol. **15**(8), 836 (2000).
[20] P. M. Te. Riele, G. Rijnders, and D. H. A. Blank, "Ferroelectric devices created by pressure modulated stencil deposition," Appl. Phys. Lett. **93**(23), 233109 (2008).
[21] M. Dekkers, M. D. Nguyen, R. Steenwelle, P. M. T. Riele, D. H. A. Blank, and G. Rijnders, "Ferroelectric properties of epitaxial Pb(Zr, Ti)O-3 thin films on silicon by control of crystal orientation," Appl. Phys. Lett. **95**, 012902 (2009).
[22] M. Dekkers, H. Boschker, M. van Zalk, M. Nguyen, H. Nazeer, E. Houwman, and G. Rijnders, "The significance of the piezoelectric coefficient d(31,eff) determined from cantilever structures," J. Micromech. Microeng. **23**, 025008 (2013).

This article is copyrighted as indicated in the article. Reuse of AIP content is subject to the terms at: http://aplmaterials.aip.org/about/rights_and_permissions Downloaded to IP: 130.89.23.40 On: Wed, 25 Mar 2015 20:47:14